

PySubdiv 1.0: open-source geological modelling and reconstruction by non-manifold subdivision surfaces

Mohammad Moulaeifard¹, Simon Bernard¹, Florian Wellmann¹

¹Computational Geoscience and Reservoir Engineering department, RWTH Aachen University, 52062 Aachen, Germany

5 Correspondence to: Mohammad Moulaeifard (mohammad.moulaeifard@cgr.rwth-aachen.de)

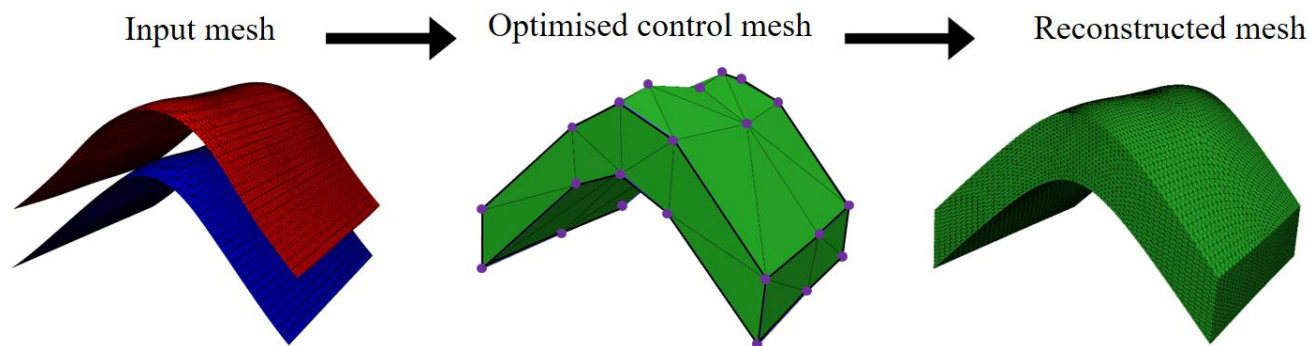


Figure 1: PySubdiv generates a watertight control mesh based on the input mesh and reconstructs it using the non-manifold subdivision surface method. The reconstructed mesh can be managed by the vertices of the control mesh (purple vertices).

Abstract.

10 Sealed geological models are commonly used as an input to process simulations, for example, in hydrogeological or
geomechanical studies. Creating these meshes often requires tedious manual work – and it is, therefore, difficult to adjust a
once-created model. In this work, we propose a flexible framework to create and interact with geological models using explicit
surface representations. The essence of the work lies in the determination of the control mesh and the definition of semi-sharp
creases values, which, in combination, enable the representation of complex structural settings with a low number of control
15 points. We achieve this flexibility through the adaptation of recent algorithms from the field of computer graphics to the
specific requirements of geological modelling, specifically the representation of non-manifold topologies and sharp features.
We combine the method with a **particle** swarm optimisation (**PSO**) approach to enable the automatic **optimisation** of vertex
position and crease sharpness values. The result of this work is implemented in an open-source software (PySubdiv) for
reconstructing geological structures while resulting in a model which is (1) sealed/watertight, (2) controllable with a control
20 mesh, and (3) topologically similar to the **input** geological structure. Also, the reconstructed model may include a fewer number
of vertices compared to the input geological structure, which results in reducing the cost of modelling and simulation. In

addition to enabling a manual adjustment of sealed geological models, the algorithm also provides a method for the integration of explicit surface representations in inverse frameworks and the consideration of uncertainties.

25 **1 Introduction**

Parametric surface-based representation is one of the major approaches to the surface representation of geological objects (De Paor 1996, Farin and Hamann 1997, De Kemp 1999). Several studies considered a surface-based approach in geological modelling since the outstanding features of the structure, e.g. heterogeneity, are explicitly demonstrated by the surfaces of the boundary without depending on grid cells (Jacquemyn et al. 2019, Moulaeifard et al. 2023). It is worth mentioning that Jacquemyn et al. (2019) comprehensively investigate the advantages of surface-based modelling compared to grid-based representation. Botsch et al. (2010) consider NURBS (Non-Uniform Rational B-Splines) and subdivision surfaces as two major methods of parametric surface-based representation for generating controllable free-form surfaces. Subdivision surfaces convert an initial mesh (control mesh) to a smooth mesh by successive refinements until the final mesh is sufficiently fine. The final smooth mesh is a controllable free-form surface which can be controlled easily by the control points (vertices of the initial mesh). Although both NURBS and Subdivision surfaces produce controllable free-form surfaces, subdivision surfaces give freedom from topological limitations, whereas NURBS underscore the smooth manipulation of the model (Cashman 2010).

Previous studies of geological modelling have dealt with NURBS (Paluszny et al. 2007, Börner et al. 2015, Jacquemyn et al. 2019). However, NURBS surfaces suffer from two limitations: (1) for generating a model with complex topology, several NURBS patches have to be stitched together, which leads to difficulty in modelling, and (2) modification of NURBS surfaces is challenging in the complex cases since NURBS surfaces are based on grid structures (DeRose et al. 1998, Sederberg et al. 2008, Botsch et al. 2010)

Although extensive research has been carried out on exploiting NURBS for geological and reservoir modelling, researchers have not considered subdivision surfaces in much detail. Lévy and Mallet (1999) and Mallet (2002) investigate the subdivision surface method, which exploits discrete smooth interpolation (D.S.I) as the refinement scheme at each iteration. In their approach, all vertices (except the control vertices) are free to move in each iteration since D.S.I is a discrete fairing method. Although their work deserves appreciation, they mention that the formal proof of the convergence of the series of recursively refined meshes is an open question; however, it can be observed experimentally. Also, they do not investigate the compatibility of subdivision surfaces for the structures with non-manifold topologies, which is broadly observed in complex geological and reservoir modelling, e.g. connection between faults and horizons, channel intersection, and hierarchical layered structures. In this paper, we focus on the non-manifold subdivision surface method based on the Loop algorithm, in which the convergence of the series of refined meshes is formally proved (Loop 1987).

One of the typical examples of non-manifold surfaces in geological modelling is where several faces of the mesh share one edge (Fig. 2). Representations of non-manifold structures require complex algorithms (Rossignac & Cardoze, 1999). The lack of supporting non-manifold surfaces is one of the limitations of classical subdivision surfaces. Ying and Zorin (2001) modified the subdivision surfaces algorithm and made it compatible with the non-manifold topology which is implemented in the core of PySubdiv.

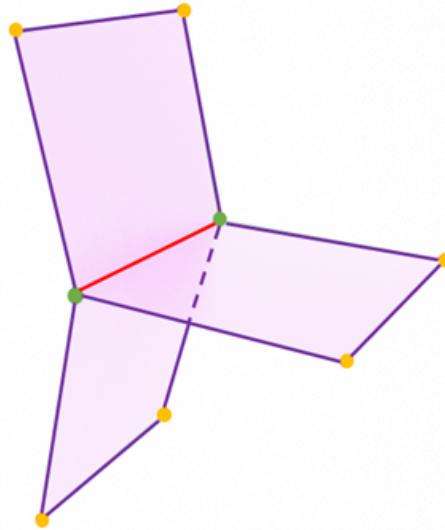


Figure 2: A common example of a non-manifold topology in geological modelling; multiple faces share one edge. Non-manifold vertices (green) and edge (red).

Classic subdivision surface algorithms tend to generate smooth surfaces. However, complex geological structures inherently consist of creases and corners (e.g., sharp fault bend), which require modified subdivision algorithms. Subdivision surfaces with the semi-sharp creases approach generate creases on the mesh by increasing the resistance of the vertices to the smoothing procedure. In practice, the resistance of the vertices can be created by applying the crease sharpness value to the edges consisting of the respective vertices. The higher the crease sharpness value of the edge is, the sharper the creases on the structure. It is worth mentioning that PySubdiv exploits the semi-sharp creases for a better representation of the creases of complex geological structures.

Furthermore, the subdivision surfaces are used for reconstruction by fitting smooth surfaces to mesh or dense point cloud data (Ma et al. 2015). The goal of reconstruction in this paper is to generate the control mesh that gives control over the reconstructed mesh with a few numbers of control points (Fig. 1). In other words, the reconstructed mesh not only is fitted to the input mesh but also can be controlled by vertices of the control mesh. Moulaeifard et al. (2023) investigate the reconstruction of geological structures by non-manifold subdivision surfaces. However, they manually fit the smooth surfaces to the input data, which is a

75 time-consuming process in complex geological structures. This paper presents the automatic reconstruction of geological structures which is implemented in the PySubdiv.

The structure of the control mesh is based on two critical variables: (1) the position of the control points and (2) the crease sharpness value of each edge. Therefore, for fitting the smooth mesh to input data, the position of the control points and crease sharpness values have to be set. Several researchers have studied the simplification method to estimate the control mesh from the input mesh (Hoppe et al. 1994, Suzuki et al. 1999, Wu et al. 2017). However, Ma et al. (2015) advise exploiting the distinguished features of the input mesh instead of the simplification method since simplification would be time-consuming for structures with complex topology. It is worth mentioning that extensive research has been carried out on exploiting the key features of the input mesh for generating the control mesh; Ma et al. (2015) use the umbilics and ridges. Also, Marinov and Kobbelt (2005) and Kälberer et al. (2007) consider the curvatures for generating the control mesh.

85 After estimating the control mesh, we have to optimise the control mesh to find the best fit to input mesh. Wu et al. (2017) investigate automatic fitting to solve the optimisation problem by using the augmented Lagrangian method. They show that their method provides significant gains over previous works, e.g. Marinov and Kobbelt (2005), by generating the reconstructed mesh with fewer control points while consisting of comparable errors. Therefore, for the sake of efficiency, PySubdiv makes use of the automatic reconstruction method proposed by Wu et al. (2017), which is explained in section 2.4. The final reconstructed structure is controllable by control points, sealed (or watertight), and topologically similar to the input model.

90 To date, there is no practical software to generate and manipulate sealed geological models using subdivision surface approaches. We attempt to close this gap with the approach described in this paper and the implementation in the accompanying software package PySubdiv. This study investigates the advantages and limitations of PySubdiv for the modelling and reconstruction of geological and reservoir structures with a case study. Also, PySubdiv can export the final files as 3D objects based on common object formats, e.g. obj, which can be read by most computer graphics and meshing software.

95 2 Methods

The core functionality of PySubdiv consists of four fundamental parts, which are investigated in the following section: (1) subdivision surface algorithm, (2) modelling with semi-sharp creases, (3) supporting non-manifold topology, and (4) automatic reconstruction.

100 2.1 Subdivision surface algorithm

The subdivision surface algorithm refines the input (control) mesh to generate the final desirable mesh based on mathematical rules (Halstead et al. 1993, Reif 1995, Stam 1998, Peters 2015). Subdivision surfaces follow two steps at each refinement: (1) *splitting* step, which includes implementing the new vertices on the surface, and (2) *averaging* step for updating the location of the vertices. There are several subdivision surface schemes based on different criteria, e.g. type of input mesh (triangular or

105 quad) and the approach for refinement. Loop Scheme (Loop 1987) is one of the common subdivision schemes for triangular meshes which is already implemented in PySubdiv. In the following, the Loop algorithm is explained.

2.1.1 Loop subdivision scheme

110 **Loop (1987)** defines the loop algorithm to generate smooth surfaces for triangular meshes by using splitting and averaging steps in each refinement stage. In the splitting step, a new vertex is inserted on the midpoint of each edge (blue vertex in **Fig. 3**), which results in the splitting of each triangle of the control mesh into four triangles (Fig. 3).

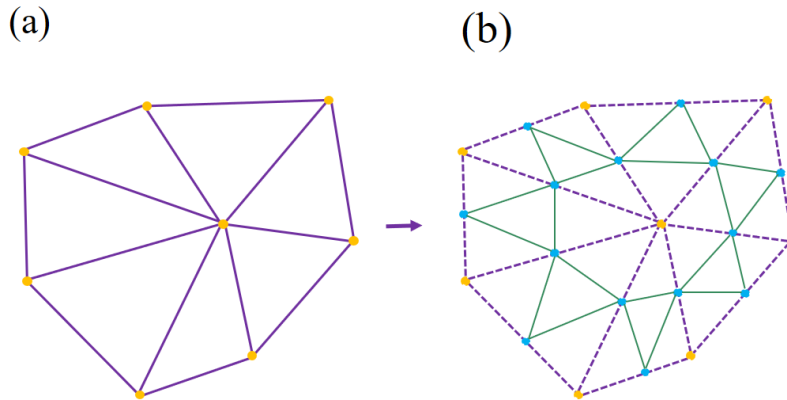


Figure 3: Splitting step of Loop scheme; (a) The control mesh; (b) Splitting each triangle into four by inserting new vertices (yellow vertices) on the mid of each edge.

115 Updating the position of the *existing* and *midpoint* vertices (yellow and blue vertices) is the averaging step of the Loop scheme (Fig. 4). To determine the new position of the *existing* vertex (q) with m adjunct vertices ($r_1, r_2, r_3, \dots, r_k$) **the** Loop scheme proposes (Fig. 4a):

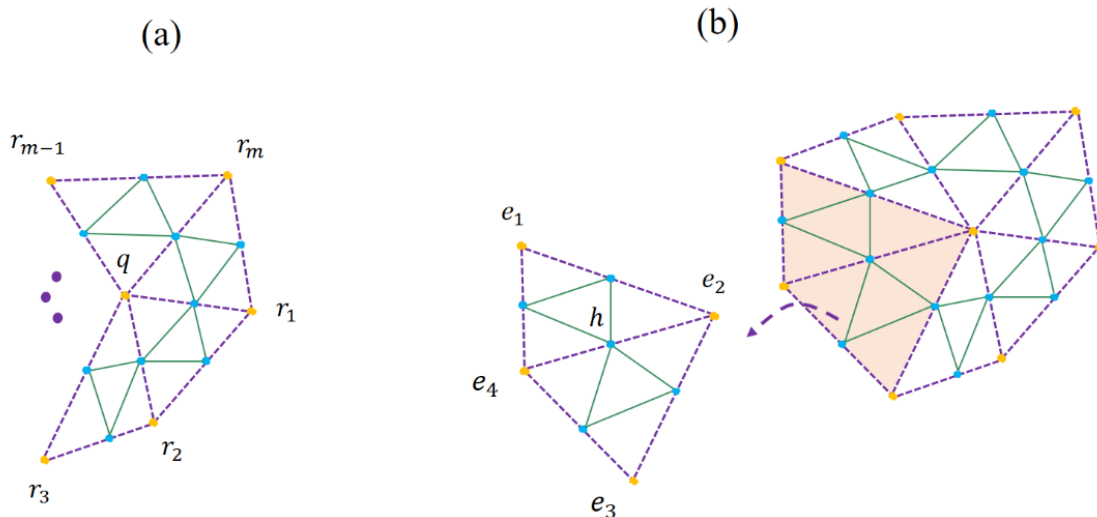
$$q_{new} = q * (1 - m\beta) + \beta \sum_1^m r_m, \quad (1)$$

where

120
$$\beta = \frac{1}{m} \left(\frac{5}{8} - \left(\frac{3}{8} + \frac{1}{4} \cos \frac{2\pi}{m} \right)^2 \right). \quad (2)$$

Also, to compute the new location of the *midpoint* of an edge (h) enclosed by four existing vertices (e_1, e_2, e_3, e_4) the Loop algorithm use (Fig. 4b):

$$h = \frac{1}{8} (e_1 + e_3) + \frac{3}{8} (e_2 + e_4). \quad (3)$$



125 **Figure 4: Averaging step of generating the smooth surface by Loop subdivision scheme; (a) Updating the position of the existing**
vertices; (b) Updating the position of the new midpoint vertices.

2.1.2 Piecewise Smooth Subdivision Surfaces

Representation of the objects consisting of sharp features by smooth subdivision algorithms leads to unsatisfactory results.

130 Hoppe et al. (1994) propose to add new rules for the representation of the creases and corners to the Loop subdivision scheme
in which the new location of the vertex v depends on the number of connected sharp edges as represented in Table 1 (DeRose
et al. 1998).

Table 1

135 The rules for updating the positions of vertices connected to sharp edges based on piecewise smooth subdivision surfaces (DeRose et al.
1998).

Number of sharp edges connected to the vertex v	The vertex v is called	The rule for updating the position of the v_{new}
one edge	dart	smooth subdivision rules (section 2.1.1)
Two edges ($v_j v$ and $v v_k$) where the v_j and v_k are two adjacent vertices connected to v by sharp edges	crease	$v_{new} = \frac{v_j + 6v + v_k}{8}$ (crease rule)
\geq three edges	corner	$v_{new} = v$ (corner rule)

The piecewise subdivision surface method presents an acceptable solution for generating the sharp regions of the model. However, in complex geological modelling, it is vital to model the semi-sharp regions which are not quite sharp.

140 **2.2 Modeling with semi-sharp creases**

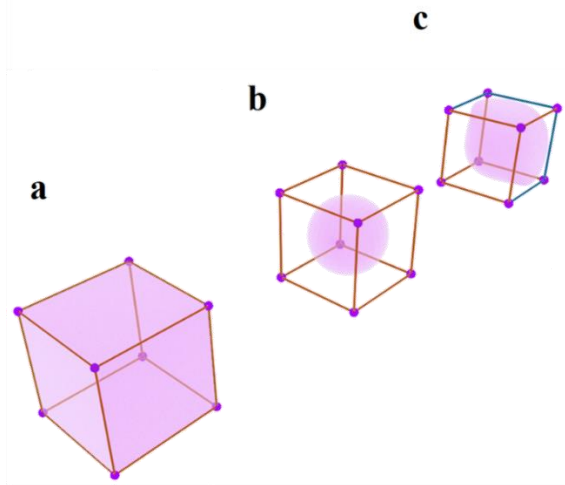
The creases and corners can be made by considering the crease sharpness values for the edges of the control mesh (Fig. 5). This value can be between zero to one, which indicates zero and infinite sharpness, respectively. Modelling different geometric objects become flexible by regulating crease sharpness. As mentioned in section 2.1.2, Hoppe et al. (1994) define the new rules for generating sharp regions during the subdivision procedure. DeRose et al. (1998) generalize the method of Hoppe et al. (1994) for updating the position of the vertices based on semi-sharp subdivision surfaces (Table 2).

Table 2

The rules of semi-sharp creases scheme for updating the positions of vertices (DeRose et al. 1998).

Number of adjacent sharp edges	The rule for updating the position of the vertex
0 or 1	smooth subdivision rules (section 2.1.1)
> 2	corner rule of Table 1
2	crease rule of Table 1

150 Fig. 5a represents the control mesh with eight control points (red vertices). Also, Fig. 5b shows the final smooth mesh after applying three times subdivision surfaces when all edges of the control mesh have no crease sharpness values. However, Fig. 5c represents the effect of the resistance of three sharp edges to the smoothing procedure (black edges, with crease sharpness values equal to one).



155 **Figure 5: Generating creases on a mesh by applying three times subdivision surface algorithm; (a) Control mesh (b); All edges of the control mesh are smooth edges (red edges); (c) Four edges are crease edges (blue edges), and nine edges are smooth (red edges).**

2.3 Supporting non-manifold topology

Non-manifold topologies are extensively observed in complex geological and reservoir modelling. Fig. 6 represents the surface intersections as a common example of non-manifold topology in geological modelling where multiple faces are shared by one edge (e.g., the intersection of different faults or intersections between a horizon and a fault).

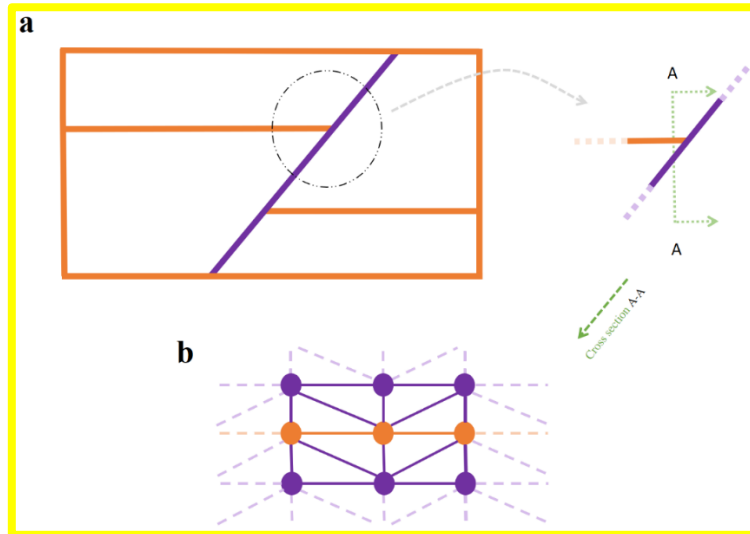


Figure 6: (a) A schematic representation of the intersection between a fault and a layer; (b) Mesh structure of the surface intersection includes the simple singular vertices (brown circles).

The classic subdivision surfaces can not support non-manifold topology since there is at least one irregular vertex or/and edge. Ying and Zorin (2001) propose the non-manifold subdivision surface algorithm, which supports a wide variety of non-manifold topology problems. A full explanation of this method is beyond the scope of this paper, and in the following, we mention part of their work which is practical in geological modelling. However, Moulaeifard et al. (2023) extensively investigated non-manifold subdivision surfaces for geological and reservoir modelling with multiple examples.

Ying and Zorin (2001) categorize the vertices of the mesh into three types and define the rule for updating the position of vertices (Table 3); (1) regular vertices, (2) simple singular non-manifold vertices that are connected only to two neighbourhood vertices by two shared non-manifold edges (Fig. 7) and, (3) complex singular non-manifold vertices which are the other non-manifold vertices. PySubdiv exploits the non-manifold subdivision surfaces for geological modelling.

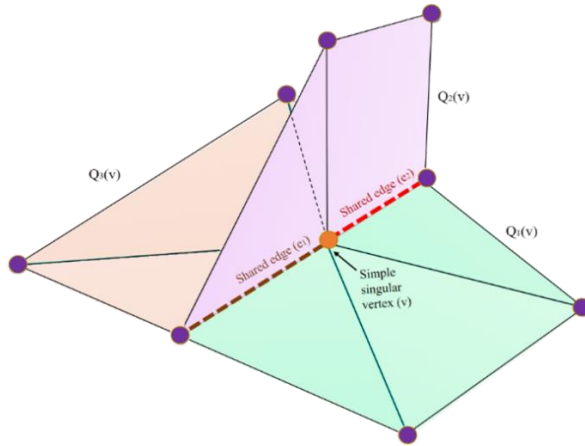


Figure 7: A representation of simple singular vertex (v) (orange vertex)

Table 3

The rules for updating the position of the vertices based on the non-manifold subdivision surface algorithm (Ying and Zorin 2001).

Vertex type	The rule for updating the position of the vertices, including non-manifold vertices
Regular (manifold)	standard Loop algorithm
simple singular	cubic B-spline subdivision algorithm. For more details, please check Moulaeifard et al. (2023)
complex singular	corner rule of Table 1 (vertex remains fixed)

2.4 Automatic reconstruction

The geological model can be constructed by various methods, e.g. marching cube from the implicit model. As mentioned in Section 1, the goal of surface reconstruction in this paper is to make the geological model manageable with a few numbers of control points (of the control mesh). In order to reconstruct the input mesh, first, the control mesh should be estimated based on the salient features of the input mesh (e.g., the location of minima, maxima, and saddle points). Exploiting the salient features of the input mesh leads to preserving the critical features of the input mesh (Ma et al. 2015). Then, the location of the control points and crease sharpness values of the edges are optimized to find the best fit of the reconstructed and input meshes.

190 It is worth mentioning that applying the subdivision surface algorithm to the watertight control mesh results in a watertight
reconstructed mesh. Fig. 8 represents the general workflow of the reconstruction process of an anticlinal structure. The input
mesh contains two triangulated surfaces which are generated by GemPy software (de la Varga et al. 2019). In order to obtain
the initial control mesh, vertices on the input mesh are extracted (purple spheres) to generate the edges, faces and, finally, a
watertight initial control mesh. The initial control mesh runs through the optimisation process to be optimised. The
195 reconstructed mesh is generated by applying the subdivision surface algorithm to the optimised control mesh.

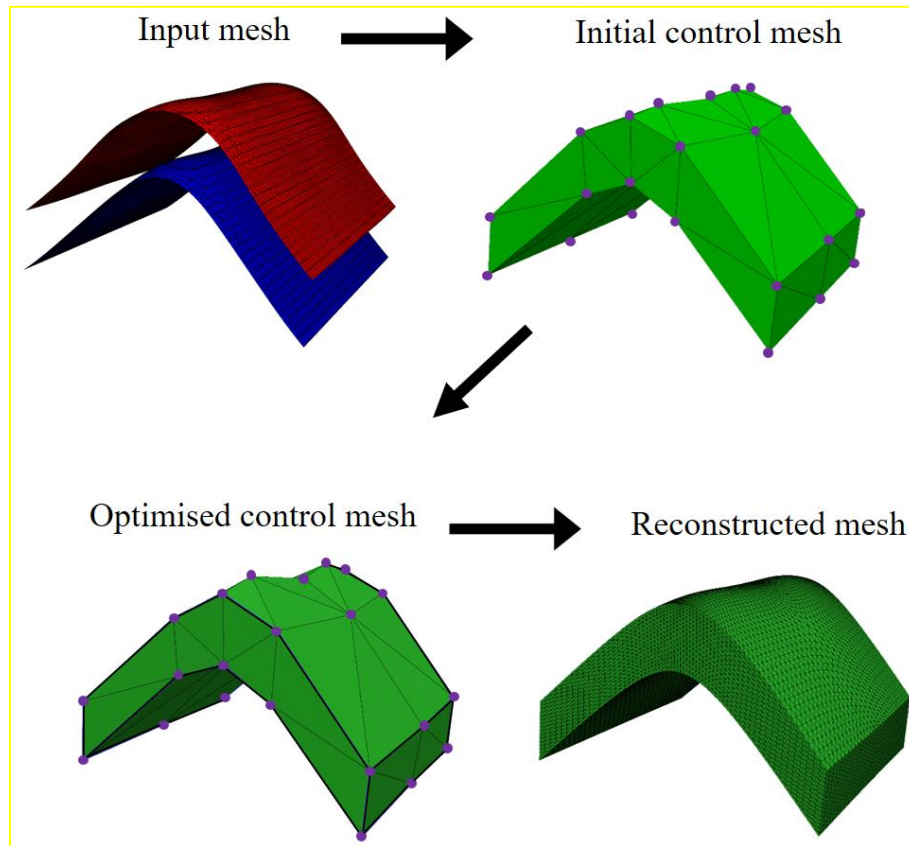


Figure 8: General workflow of subdivision surface fitting with an example of an anticlinal structure.

200 Also, the following conceptualized approach can be mentioned for the reconstruction process (Fig. 9):
A noisy input mesh \mathcal{M} (black curve), e.g. a rough geological interface, is generated from laser scanning or geophysical
measurements. A coarse control mesh K (orange curve) is generated based on the features of the input mesh (e.g., minima and
maxima), which contains the control points v_i . An unfitted subdivision surface S_K is generated based on the control mesh. On
the subdivision surface, $s(v_i)$ indicates the position of vertices v_i after subdivision. Hence, the distances d_i between $s(v_i)$ and
205 the input surface can be calculated by projecting the normal from the input mesh or finding the closest vertices (Marinov and

Kobbelt 2005). Finally, the distance is minimized by repositioning the control points v_i and setting the crease sharpness value to the edges.

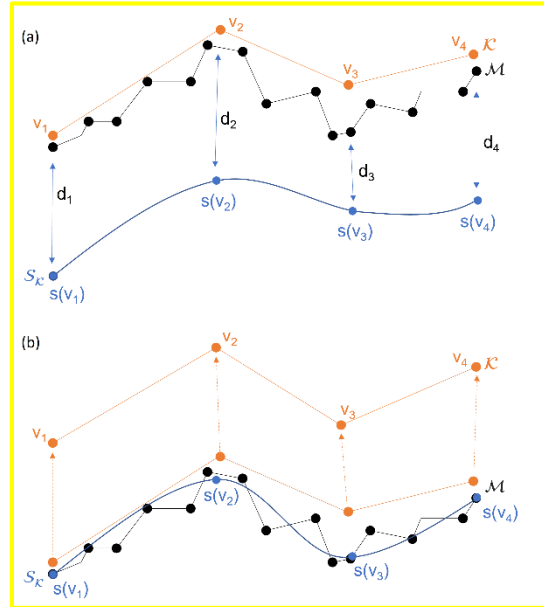


Figure 9: Synthesized and conceptualized approach for surface fitting with subdivision surfaces.

210

Wu et al. (2017) investigate the automatic reconstruction by solving an optimisation problem. In their method, the positions of the control points and the crease sharpness value of each edge repeatedly change until the best fit is achieved. In both manual and automatic methods, the first step is the estimation of the control points (c) with outstanding features of the input geological mesh, e.g. local maxima and minima. PySubdiv proposes some critical points of the input mesh as suitable candidates for the generation of the control mesh. However, it is always possible to arbitrarily select a set of control points. Then PySubdiv used the Delaunay triangulation approach to generate the initial control mesh. The second step is the reconstruction through optimising the location of control points and crease sharpness value for each edge of the control mesh to find the best fit of the reconstructed mesh to the input mesh.

215

220

Given the input geological mesh consisting of m vertices $q = \{q_1, q_2, q_3, \dots, q_m\}$, the control mesh consisting of n vertices $c = \{c_1, c_2, c_3, \dots, c_n\}$ and m edges with the crease sharpness values $h = \{h_1, h_2, h_3, \dots, h_m\}$. The goal is to minimize the vector k , which indicates the difference between q and the projection of q onto the reconstructed (subdivided) mesh. Hoppe et al. (1994) mention that each vertex of the *reconstructed* mesh can be approximated as an affine combination of control points (c). Therefore the foot point vector of the q on the reconstructed mesh can be approximated as $f(h) c$ where $f(h)$ is a matrix depend on h . Therefore, the optimisation problem can be represented by

225

$$\min\{\|k\|\}, \quad (4)$$

subject to $k = q - f(h)c$. Wu et al. (2017) offer the following augmented Lagrangian function for solving Eq. (4) by using the augmented Lagrangian approach:

$$\mathcal{L}(c, h, k; \lambda) = \|k\| + \langle \lambda, (k - (q - f(h)c)) \rangle + \frac{b}{2} \|k - (q - f(h)c)\|^2, \quad (5)$$

where λ is the Lagrange multiplier, \langle, \rangle is the vector dot product operator, and b is a positive number. The following optimisation algorithm (Algorithm 1) is used for solving Eq. (5), which includes solving three sub-problems respecting c, h, k at each iteration.

230

Algorithm 1 Reconstruction by semi-sharp subdivision surfaces based on (Wu et al. 2017)		
Input	ϵ_0	<i>Error threshold</i>
	$h^{(0)}$	<i>Intial CSV of the edges of the control mesh</i>
	$c^{(0)}$	<i>Intital position of the estimated control points</i>
	$\lambda^{(0)} = 0$	<i>Initial value for Lagrangian multiplier</i>
	$k^{(0)} = 0$	<i>Initial value for k</i>
	i, b	<i>Iteration , Coefficent</i>
<p>while $\epsilon > \epsilon_0$ and $i < \text{max-iterations}$ do</p> <p>compute $c^{(i+1)}, h^{(i+1)}, k^{(i+1)}$ (assume $c^{(i+1)} = c^{(i)}, h^{(i+1)} = h^{(i)}, k^{(i+1)} = k^{(i)}$),</p> <p>$c^{(i+1)} = \arg \min \mathcal{L}(c, h^{(i+1)}, k^{(i+1)}; \lambda^{(i)}) \rightarrow \text{Eq (6)},$</p> <p>$h^{(i+1)} = \arg \min \mathcal{L}(c^{(i+1)}, h, k^{(i+1)}; \lambda^{(i)}) \rightarrow \text{Eq (7)},$</p> <p>$k^{(i+1)} = \arg \min \mathcal{L}(c^{(i+1)}, h^{(i+1)}, k; \lambda^{(i)}) \rightarrow \text{Eq (10)},$</p> <p>update the Lagrange multiplier:</p> <p>$\lambda^{(i+1)} = \lambda^{(i)} + b * (k^{(i+1)} - (q - f(h^{(i+1)}) c^{(i+1)})),$</p> <p>$\epsilon < \ c^{(i+1)} - c^{(i)}\ ^2,$</p> <p>$i = i + 1,$</p> <p>end while</p>		

I) Sub-problem with respect to c : the position of the control points c can be calculated in each iteration of optimisation by solving Eq. (6), which is a *linear* problem:

235

$$\min_c \left(\langle \lambda, (k - (q - f(h) c) \rangle + \frac{b}{2} \|k - (q - f(h) c)\|^2 \right). \quad (6)$$

II) Sub-problem with respect to h : the crease sharpness values, h , in each iteration can be captured by adapting particle swarm optimisation (PSO) (Kennedy and Eberhart 1995) :

$$\min_h \left(\langle \lambda, (k - (q - f(h) c) \rangle + \frac{b}{2} \|k - (q - f(h) c)\|^2 \right). \quad (7)$$

240 III) Sub-problem with respect to the k : k can be calculated in each iteration by

$$\min_k \left(\|k\| + \langle \lambda, (k - (q - f(h) c) \rangle + \frac{b}{2} \|k - (q - f(h) c)\|^2 \right). \quad (8)$$

Calculating Eq. (8) results in the following:

$$1 + \lambda + b \left(k - (q - f(h) c) \right) = 0, \quad (9)$$

finally, k can be computed by

$$245 \quad k = q - f(h) c - \frac{(1+\lambda)}{b}. \quad (10)$$

3 CORE of PySubdiv

As mentioned in section 2, the core functionality of PySubdiv includes (1) subdivision surface algorithm, (2) modelling with semi-sharp creases, (3) supporting non-manifold topology, and (4) automatic reconstruction. PySubdiv is written with an object-oriented approach using Python programming language (Rossignac and Cardoze 1999). Also, PySubdiv exploits different varieties of open-source external libraries which are integrated into the core. Table 4 represents the main external libraries implemented in PySubdiv.

Table 4

The main external libraries implemented in PySubdiv.

	Library	Explanation
1	PyVista	Interactive 3D graphics application programming interface (Sullivan and Kaszynski 2019)
2	Numpy	Well-organise numerical computations (Van Der Walt et al. 2011)
3	PySwarms	A toolkit for particle swarm optimisation (PSO) (Miranda 2018)
4	Scipy	Scientific computing (Virtanen et al. 2020)

255

3.1 Step-by-Step Workflow for the Reconstruction of a Geological Mesh by PySubdiv

(I) Generating the Control Mesh (Semi-Automatic)

PySubdiv accepts the structures with triangle mesh, while the input mesh can be generated by any arbitrary method (e.g. implicit or explicit). Also, the input mesh can be either watertight or non-watertight. If the input mesh is not triangulated,

260 PySubdiv can convert the input mesh to the triangle mesh by using the triangulate function of the PyVista library (Sullivan and Kaszynski 2019).

The estimation of the position and number of control points is the key stage in reconstruction which leads to the generation of the watertight modelling by providing the control points at surface intersections. PySubdiv offers some candidates to the user based on the features of the input geological structure, e.g. minima, maxima and boundaries. However, it is always possible
265 for the user to select or generate the control points based on the requirements for the interpretation. For example, the geological models generated based on real data may be associated with uncertainties (Wellmann and Caumon 2018). The user can consider some control points at the suspicious locations regardless if the locations are on the boundary or body part of the layer.

In order to show the general workflow of generating control mesh in PySubdiv, an anticlinal structure model is investigated. Figure 10 represents the GUI window of PySubdiv containing the anticline model (two non-watertight surfaces) which is
270 generated by Gempy (de la Varga et al. 2019). It is worth mentioning that watertight or non-watertight meshes can be imported as the input mesh. All of the elements inside the GUI are explained in the appendix of this paper.

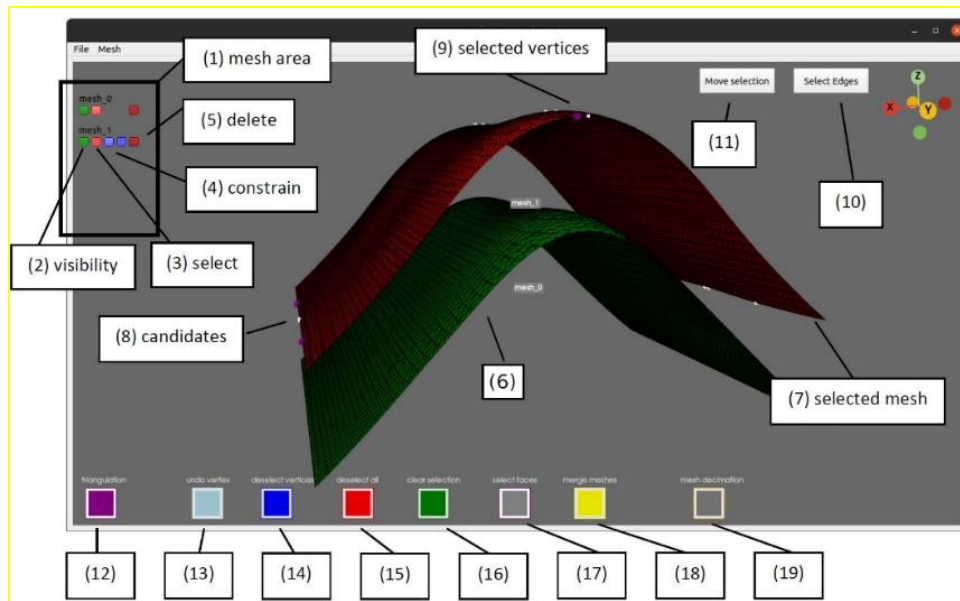


Figure 10: The GUI of PySubdiv allows the user to construct the control mesh for the (geological) model. The important GUI elements are labelled and explained in the following.

275

First, the top mesh is selected (the colour changes from green to red after selection). Then, the control points should be chosen among the vertices of the selected mesh (Fig. 11a). The individual points can be selected by pressing the “P” button on the keyboard while the mouse cursor hovers above them. In this example, the maximal points on the anticline axis have been chosen, as well as an additional point in the centre. Three points on the flanks have been sampled to support the control mesh
280 at the turning point. Further important points lie in the corner of the mesh. The next step is to triangulate the selected points.

Pressing the triangulation button (12) starts the triangulation. The users are asked if they want to define a polygon used as the “boundary” during the triangulation. If declined, the Delaunay algorithm is executed directly on the automatically detected boundaries. However, unwanted orthogonal faces might appear. It is worth noting that the polygon boundary for the Delaunay algorithm can be defined by the user. Finally, the triangulated control mesh is generated (Fig. 11b). Repeating the mentioned steps for the second input surface yields the second simplified surface for the control mesh.

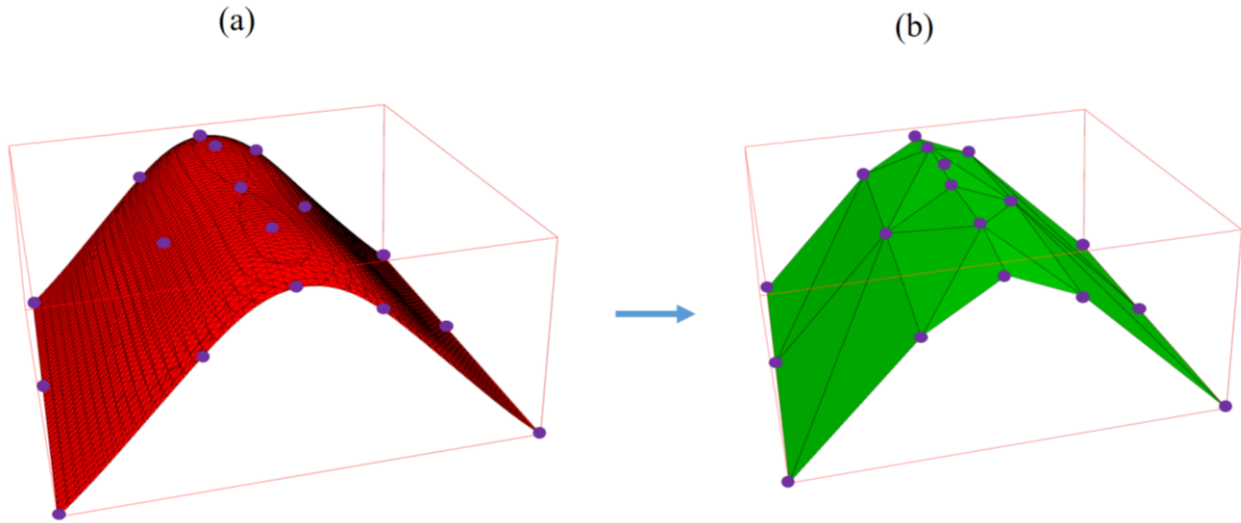


Figure 11: (a) Control points are generated based on the vertices of the input mesh; (b) Triangulated control mesh is constructed based on the control points and the Delaunay triangulation.

In order to create a watertight mesh, four additional sides should be created for the anticline model. Therefore, the boundary vertices of the two simplified surfaces are selected and triangulated. The vertices should be sampled from the simplified surfaces to generate the watertight control mesh (Fig. 12a). At the moment, the four sides must be meshed individually and then merged together. When all four sides are generated, the different meshes can be stitched together by merging. Finally, the sealed control mesh is generated and shown in (Fig. 12b).

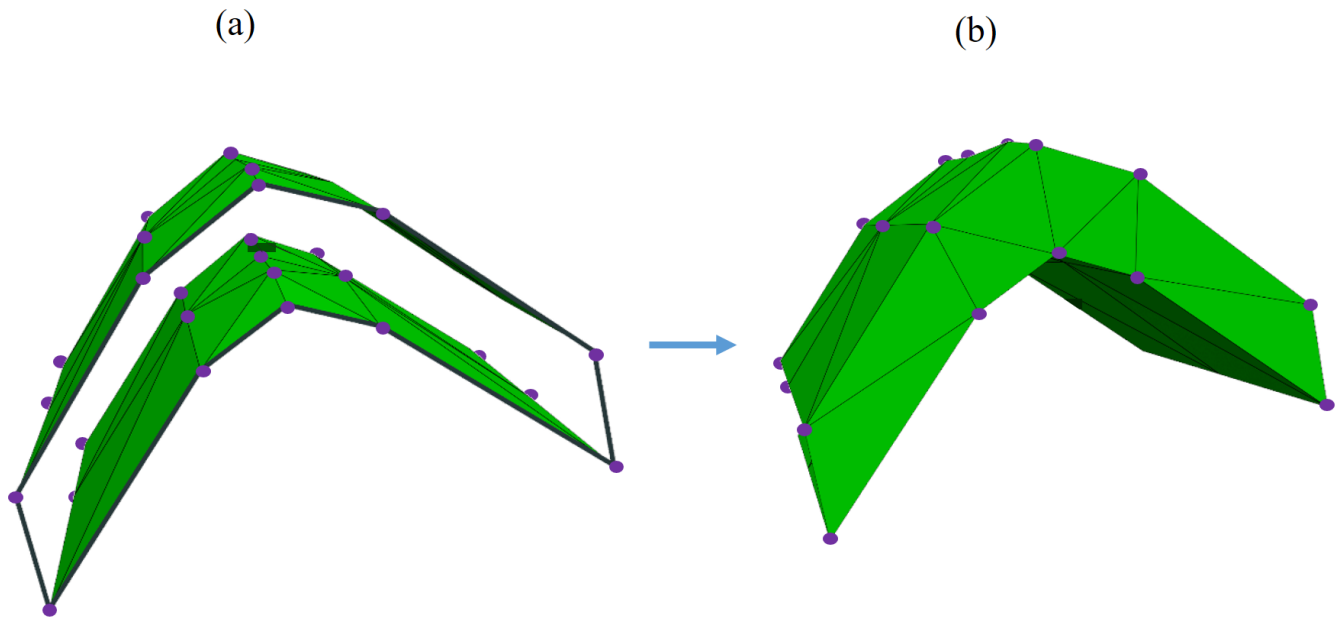


Figure 12: (a) Stitching and merging the different parts of the control mesh to make it watertight ; (b) Final watertight control mesh

300

(II) Set the Crease Sharpness Value to the Edges (automatically done by software)

The next step is to assign the crease sharpness value for each edge of the initial control mesh (Fig. 12b). Hoppe et al. (1994), Wu et al. (2017) offer to consider a threshold angle (θ_0) as a criterion for tagging the edges of the initial control mesh. For each edge, it is tagged as sharp (e.i., crease sharpness value equal to one) if the angle between the normal of two adjacent faces (θ_e) is more than the threshold angle ($\theta_e > \theta_0$). It is worth reminding that this value is just an initial estimation for crease sharpness values.

305

(III) Reconstruction (Optimisation) of Control Mesh (automatically done by software)

In the first step of optimisation, the generated (initial) control mesh and the original input meshes are imported as the input data for the reconstruction algorithm (Algorithm 1). “MeshOptimizer” class instantiates an object based on the input data, which can start the fitting process with the “optimize” method. It is worth mentioning that the final subdivided (reconstructed) mesh can be exported by applying the subdivision surface algorithm to the optimized control mesh.

310

4 Case study

As a case study, a part of Upper Rhine Graben (URG) is reconstructed by PySubdiv. URG is a long geological structure in the central part of the European Cenozoic rift system that contains geothermal energy resources. The data set of the URG consists of several different geological units (grid nodes) published by Freymark et al. (2020), which consists of 616464 individual nodes (Fig. 13). The dimensions of the original model are 292 km in the x-direction, 525 km in the y-direction and 130 km deep (z-direction).

As mentioned in section 3, the input data of PySubdiv should consist of the triangular mesh, which can be generated by any arbitrary method or software. In this case study, PyVista generates the triangular mesh from the individual grid nodes, resulting in 18 different surfaces and ten volumes.

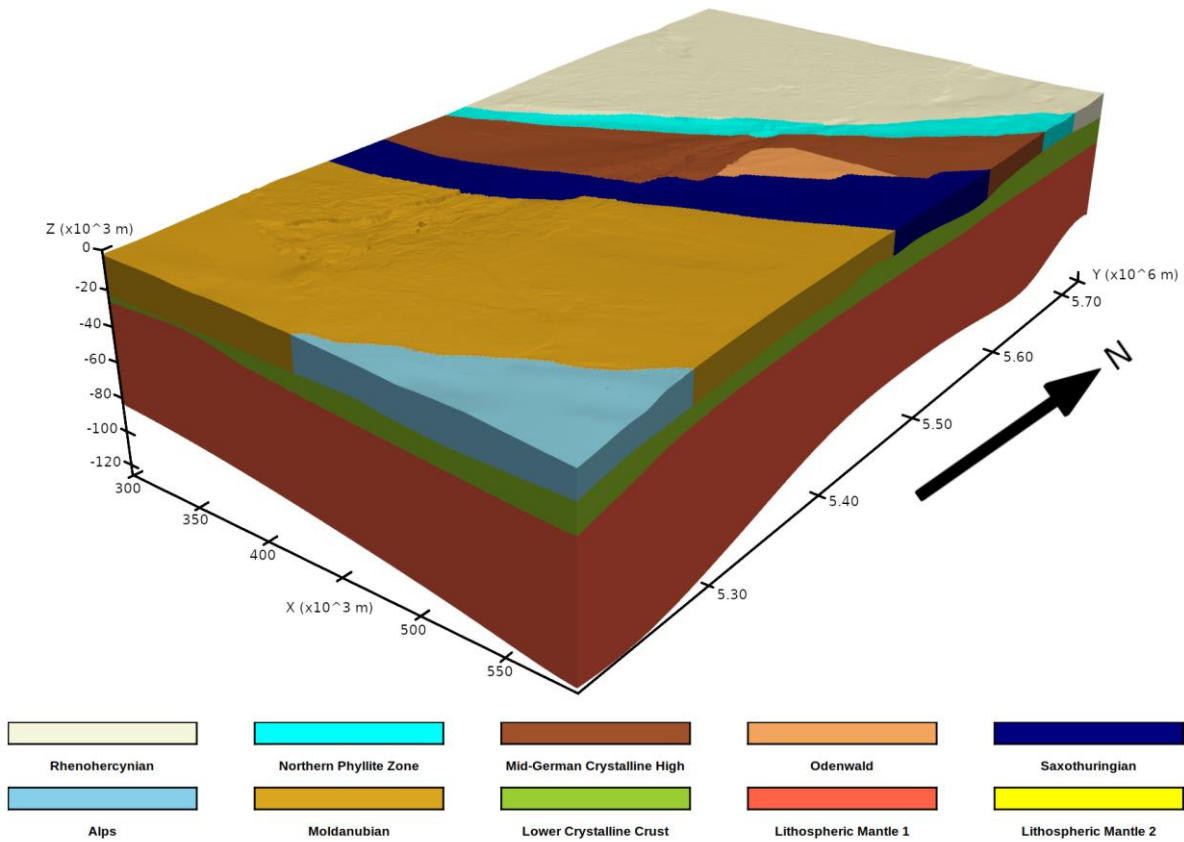


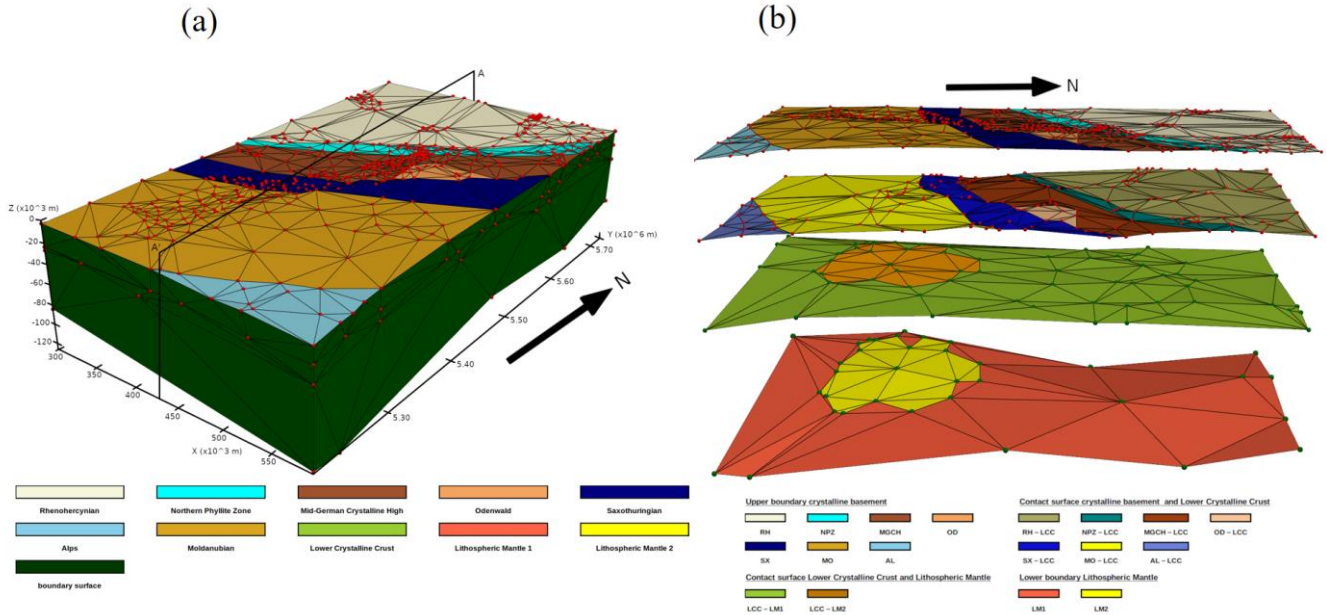
Figure 13: Grid-based representation of part of URG model which contains 616464 individual nodes and 10 different volumes generated based on the data of Freymark et al. (2020).

325

4.1 Estimation of the control mesh

The initial watertight control mesh is prepared based on the prominent features of the input mesh, such as (a) minimal and maximal points and (b) surface intersections of different layers to ensure that the final mesh is watertight. Fig. 14 represents the control mesh consisting of 832 control points distributed over 18 individual surfaces.

330 Also, the edges of the control mesh, which consist of a threshold angle of 80° (section 3.1), are considered sharp and given the crease sharpness values equal to one. Other edges are considered smooth and assigned crease sharpness values equal to zero. From our experience, exploiting the angle of 80° as the threshold angle in this case study leads to acceptable results. However, this angle can be different depending on the complexity of the model.



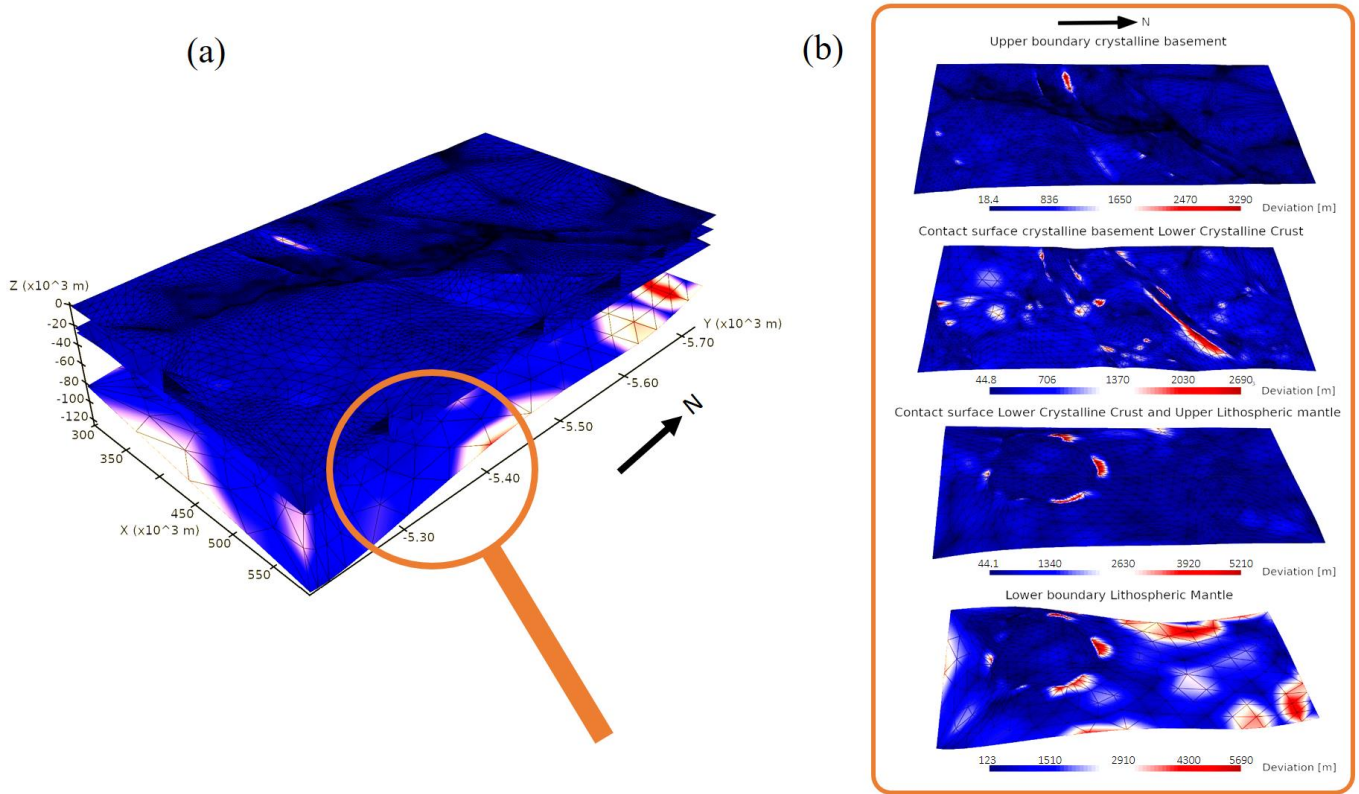
335 **Figure 14: (a) Initial and unfitted control mesh of the URG model. Surfaces are coloured concerning the different geological units. The surfaces of the Lower Crystalline Crust and the Lithosphere mantel are hidden by the boundary surface. The 832 control points are coloured in red; (b) Approximately representation of the 3D side view of the model along the profile AA'.**

4.2 Optimisation of the control mesh

340 The reconstructed mesh is generated after applying two subdivisions to the control mesh (Fig. 15). It consists of roughly 15000 vertices. In order to evaluate the reconstructed structure, the distance metric between the points of the original and the reconstruction model is computed. Red-coloured areas imply high deviations of the subdivided surface from the original model. The mean error for the whole domain is approximately $496 \text{ m} \pm 362 \text{ m}$ which is around 0.6% of the total elevation height. Areas of high error concentrate mainly in regions where two individual geological units are connected and further on the lower

345 boundary of the Lithospheric Mantle (lower boundaries of Fig. 13). On the Lithospheric Mantle, the highest errors are up to

5700 m which is around 4.75% of the total elevation (approximately 120 km). Most parts of the model consist of small deviations indicated by the dark blue colour, especially the higher elevated layers are well-fitted.



350 **Figure 15: (a) Distance map of the subdivided surfaces compared to the input mesh (Fig. 13). Red areas indicate high deviation from the original input mesh while blue areas indicate low deviation; (b) Exploded view on the distance map of the four extracted sub-horizontal layers. Distances are scaled for each layer individually to emphasize the areas of high and low errors independent of the maximal global error.**

355

360

5 Discussion

The following section discusses the advantages and limitations of PySubdiv in complex geological reconstruction.

5.1 User and PySubdiv interaction

365 PySubdiv provides a computational framework to generate meshes with limited user interaction. The control points play a key role in estimating, generating and exploiting the reconstruction mesh. The position of the control points can be estimated based on three major criteria; (1) the goal of the user for reconstruction, e.g. uncertainty analysis of the whole or specific part of the structure, (2) salient features of the input mesh, e.g. maxima, minima, and points with high curvature, and (3) surface intersections. Since the goal of the user for reconstruction, e.g. uncertainty analysis of the specific part of the structure, can not
370 be automatically recognised by the PySubdiv, the user is asked to interact with the software over the GUI to indicate the desired important locations.

However, exploiting the GUI inside the PySubdiv leads to several limitations. As mentioned in Section 3, PySubdiv uses PyVista for graphical visualization, which exploits PyQt for the GUI. Some of the PySubdiv users reported the crashes of PyQt with or without any error, especially when using Mac OS or Windows systems. The current version of PySubdiv suffers from
375 this limitation which we hope to be solved in future versions.

5.2 Challenges in generating the reconstructed mesh

PySubdiv exploits semi-sharp subdivision surfaces for the reconstruction algorithm which is used by several studies (Lavoué et al. 2007, Wu et al. 2017). However, some studies, e.g., Marinov and Kobbelt (2005), use classic subdivision surfaces for
380 reconstruction. Although using semi-sharp subdivision surfaces would reduce the number of control points, the non-linear role of crease sharpness value in reconstruction optimisation cannot be ignored since it takes the most time-consuming part of the reconstruction process. As a remedy, Powell's gradient-free method (Powell 1964) of the SciPy library (Virtanen et al. 2020) is implemented instead of PSO in pySubdiv to optimise the non-linear part of the reconstruction. However, it could not significantly reduce the time of this process.

385 Besides the crease sharpness values, it is worth mentioning that finding suitable locations for the control points based on the salient features of the input mesh is not always easy. For example, assume the geological surface contains two adjacent and approximately flat parts which come close together (Fig. 16). At first glance, this surface has no outstanding features (e.g., min, max, saddle points). However, it is necessary to consider more control points on the boundaries to distinguish the different parts of the surface during the reconstruction process (otherwise, the two different surface parts may be stitched together during
390 reconstruction). This topic is beyond the scope of this paper, and we plan to investigate it in future research.

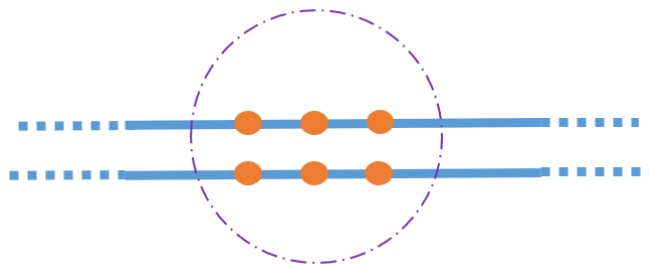


Figure 16: Distinguishing different parts of the surface by adding control points to avoid failure in the reconstruction process.

5.3 External libraries limitation

From the computational point of view, the major goal of PySubdiv is the calculation of the new location for the vertices of the control mesh based on the subdivision algorithm. Therefore, NumPy (Van Der Walt et al. 2011) and Scipy (Virtanen et al. 2020) libraries play key roles in the core of the software, which can be the source of problems when the input mesh is large, e.g. limited memory.

Although the structure of the PySubdiv is planned to avoid the generation of unnecessary big matrixes, the initial input data can also help to tackle this problem. For example, the suitable number of subdivisions is one of the key input data in reconstruction (the number of subdivisions controls the smoothness of the final mesh, which is different from the number of iterations of the optimisation process). Applying a small number of subdivisions can not guarantee the acceptable generation of smooth and semi-sharp parts of a reconstructed mesh. However, applying a large number of subdivisions not only does not make significant differences in the smoothness of the reconstructed mesh but also remarkably increases the unnecessary calculation costs since more subdivisions mean dealing with more vertices.

6 Conclusion

This study illustrated the framework (PySubdiv) to generate suitable control meshes and fitted reconstructed meshes for complex geological structures and reservoir models based on the non-manifold subdivision surface algorithm. The reconstructed mesh is watertight and topologically similar to the input mesh. Also, the control mesh consists of those control points which play a key role in the flexibility and management of the reconstructed mesh. Subdivision surfaces, unlike spline surfaces, support arbitrary topology, which gives more freedom to the user during generating the control mesh.

Appendix A: Explanation of the Elements inside the GUI (Fig. 10) for generation of the control mesh

- (1) In the mesh area, any mesh resides that is imported or created inside the GUI. The different meshes can be accessed here.
- (2) This button regulates the visibility of a mesh, helping to keep the viewer clean by disabling unnecessary meshes.
- 420 (3) This button selects a mesh allowing the user to sample the mesh vertices or edges. Selected meshes are coloured red (7).
More than one mesh can be selected at a time.
- (4) The two blue buttons can be toggled to constrain the selection to vertices on the boundary and intersection of two surfaces (left) or to minimal and maximal vertices (right) on the mesh. Constrained points are rendered white (8).
- (5) The red button deletes the mesh from the viewer.
- 425 (6) Meshes that are not selected are coloured green.
- (7) The selected mesh appears in red. Only vertices on the selected mesh can be sampled.
- (8) When a constraint is selected, candidates are shown as white points on the mesh, and only the candidates can be selected.
- (9) Selected vertices are marked in purple.
- (10) Button to toggle between edge selection and vertex selection. The current selection is cleared when the mode is switched.
- 430 (11) Button to enable the moving of selected points. Creates a widget that can be moved in space and the direction is applied to the position of the vertices/edges as a vector.
- (12) Button to triangulate between the selected mesh. In PySubdiv, a 2D Delaunay algorithm from PyVista (Sullivan and Kaszynski 2019) is implemented, which can be bounded by a polygon. Delaunay triangulation is a common method to approximate geological surfaces (Caumon et al. 2009). The polygon can be defined by the user. The order of the polygon is
- 435 important. If the order is clockwise or counter-clockwise, define the inner boundaries (holes) or the outer boundary.
- (13) Button to remove the last selected vertex from the selection.
- (14) Switch to deselection mode. Already selected vertices can be deselected by picking them again.
- (15) Deselect all current selected vertices or edges.
- (16) Clears the selected vertices, edges, and meshes.
- 440 (17) Switch to face selection mode. Selected faces can be deleted from the mesh, which is useful when triangulation creates additional faces.

(18) Merges two surface meshes together to form a watertight mesh. In order to form a watertight mesh, vertices on the intersection must be the same on both meshes.

(19) Starts the decimation of a selected mesh. The reduction factor can be set by the user.

445

Code availability

PySubdiv, is a free, open-source Python library licensed under the GNU Lesser General Public License v3.0 (GPLv3). It is hosted on the GitHub repository <https://github.com/SimBe-hub/PySubdiv> (<https://doi.org/10.5281/zenodo.6878051>)

450 Author Contributions

MM and **FW** contributed to project conceptualisation and method development. **SB** wrote and maintained the code with the help of **MM**. Also, **SB** was involved in visualising the results. **MM** prepared the manuscript with the contributions of both co-authors. **FW** provided overall project supervision and funding.

455 Acknowledgements

We would like to thank our colleagues for their support. This project has received funding from the European Institute of Innovation and Technology— Raw Materials—under grant agreements No 16258 and No 19004. We thank the developers of the Blender project for the open-source computer graphics software (<http://www.blender.org/>), which we used for rendering several figures of this paper.

460 References

- Börner, J. H., M. Bär, and K. Spitzer. 2015. Electromagnetic methods for exploration and monitoring of enhanced geothermal systems—a virtual experiment. *Geothermics* **55**:78-87.
- Botsch, M., L. Kobbelt, M. Pauly, P. Alliez, and B. Lévy. 2010. Polygon mesh processing. CRC press.
- Cashman, T. J. 2010. NURBS-compatible subdivision surfaces. Cashman, Thomas J.
- 465 Caumon, G., P. Collon-Drouaillet, C. Le Carlier de Veslud, S. Viseur, and J. Sausse. 2009. Surface-based 3D modeling of geological structures. *Mathematical Geosciences* **41**:927-945.
- De Kemp, E. A. 1999. Visualization of complex geological structures using 3-D Bézier construction tools. *Computers & Geosciences* **25**:581-597.
- de la Varga, M., A. Schaaf, and F. Wellmann. 2019. GemPy 1.0: open-source stochastic geological modeling and inversion. *Geoscientific Model Development* **12**:1-32.
- 470 De Paor, D. G. 1996. Bézier curves and geological design. Pages 389-417 *Computer methods in the geosciences*. Elsevier.
- DeRose, T., M. Kass, and T. Truong. 1998. Subdivision surfaces in character animation. Pages 85-94 *in Proceedings of the 25th annual conference on Computer graphics and interactive techniques*.
- Farin, G., and B. Hamann. 1997. Current trends in geometric modeling and selected computational applications. *Journal of Computational Physics* **138**:1-15.
- 475 Freymark, J., M. Scheck-Wenderoth, K. Bär, M. Stiller, J.-G. Fritsche, M. Kracht, and M. L. Gomez Dacal. 2020. 3D-URG: 3D gravity constrained structural model of the Upper Rhine Graben.
- Halstead, M., M. Kass, and T. DeRose. 1993. Efficient, fair interpolation using Catmull-Clark surfaces. Pages 35-44 *in Proceedings of the 20th annual conference on Computer graphics and interactive techniques*.

- 480 Hoppe, H., T. DeRose, T. Duchamp, M. Halstead, H. Jin, J. McDonald, J. Schweitzer, and W. Stuetzle. 1994. Piecewise smooth surface reconstruction. Pages 295-302 *in* Proceedings of the 21st annual conference on Computer graphics and interactive techniques.
- Jacquemyn, C., M. D. Jackson, and G. J. Hampson. 2019. Surface-based geological reservoir modelling using grid-free NURBS curves and surfaces. *Mathematical Geosciences* **51**:1-28.
- 485 Kälberer, F., M. Nieser, and K. Polthier. 2007. Quadcover-surface parameterization using branched coverings. Pages 375-384 *in* Computer graphics forum. Wiley Online Library.
- Kennedy, J., and R. Eberhart. 1995. Particle swarm optimization. Pages 1942-1948 *in* Proceedings of ICNN'95-international conference on neural networks. IEEE.
- Lavoué, G., F. Dupont, and A. Baskurt. 2007. A framework for quad/triangle subdivision surface fitting: Application to mechanical objects. Pages 1-14 *in* Computer Graphics Forum. Wiley Online Library.
- 490 Lévy, B., and J.-L. Mallet. 1999. Discrete smooth interpolation: Constrained discrete fairing for arbitrary meshes. Available on www at <http://www.loria.fr/levy/Papers/1999/s99dsi.pdf>.
- Loop, C. 1987. Smooth subdivision surfaces based on triangles.
- Ma, X., S. Keates, Y. Jiang, and J. Kosinka. 2015. Subdivision surface fitting to a dense mesh using ridges and umbilics. *Computer Aided Geometric Design* **32**:5-21.
- 495 Mallet, J.-L. 2002. Geomodeling. Oxford University Press.
- Marinov, M., and L. Kobbelt. 2005. Optimization methods for scattered data approximation with subdivision surfaces. *Graphical Models* **67**:452-473.
- Miranda, L. J. 2018. PySwarms: a research toolkit for Particle Swarm Optimization in Python. *Journal of Open Source Software* **3**:433.
- 500 Moulaeifard, M., F. Wellmann, S. Bernard, M. de la Varga, and D. Bommers. 2023. Subdivide and Conquer: Adapting Non-Manifold Subdivision Surfaces to Surface-Based Representation and Reconstruction of Complex Geological Structures. *Mathematical Geosciences* **55**:81-111.
- Paluszny, A., S. K. Matthäi, and M. Hohmeyer. 2007. Hybrid finite element–finite volume discretization of complex geologic structures and a new simulation workflow demonstrated on fractured rocks. *Geofluids* **7**:186-208.
- Peters, J. 2015. Point-augmented biquadratic C1 subdivision surfaces. *Graphical Models* **77**:18-26.
- 505 Powell, M. J. 1964. An efficient method for finding the minimum of a function of several variables without calculating derivatives. *The computer journal* **7**:155-162.
- Reif, U. 1995. A unified approach to subdivision algorithms near extraordinary vertices. *Computer Aided Geometric Design* **12**:153-174.
- Rossignac, J., and D. Cardoze. 1999. Matchmaker: Manifold Breps for non-manifold r-sets. Pages 31-41 *in* Proceedings of the fifth ACM symposium on Solid modeling and applications.
- 510 Sederberg, T. W., G. T. Finnigan, X. Li, H. Lin, and H. Ipson. 2008. Watertight trimmed NURBS. *ACM Transactions on Graphics (TOG)* **27**:1-8.
- Stam, J. 1998. Evaluation of loop subdivision surfaces. *in* SIGGRAPH'98 CDROM Proceedings. Citeseer.
- Sullivan, C., and A. Kaszynski. 2019. PyVista: 3D plotting and mesh analysis through a streamlined interface for the Visualization Toolkit (VTK). *Journal of Open Source Software* **4**:1450.
- 515 Suzuki, H., S. Takeuchi, and T. Kanai. 1999. Subdivision surface fitting to a range of points. Pages 158-167 *in* Proceedings. Seventh Pacific Conference on Computer Graphics and Applications (Cat. No. PR00293). IEEE.
- Van Der Walt, S., S. C. Colbert, and G. Varoquaux. 2011. The NumPy array: a structure for efficient numerical computation. *Computing in science & engineering* **13**:22-30.
- Virtanen, P., R. Gommers, T. E. Oliphant, M. Haberland, T. Reddy, D. Cournapeau, E. Burovski, P. Peterson, W. Weckesser, and J. Bright. 520 2020. SciPy 1.0: fundamental algorithms for scientific computing in Python. *Nature methods* **17**:261-272.
- Wellmann, F., and G. Caumon. 2018. 3-D Structural geological models: Concepts, methods, and uncertainties. Pages 1-121 *Advances in Geophysics*. Elsevier.
- Wu, X., J. Zheng, Y. Cai, and H. Li. 2017. Variational reconstruction using subdivision surfaces with continuous sharpness control. *Computational Visual Media* **3**:217-228.
- 525 Ying, L., and D. Zorin. 2001. Nonmanifold subdivision. Pages 325-569 *in* Proceedings Visualization, 2001. VIS'01. IEEE.